ORIGINAL COMMUNICATION

Glucose metabolism in nine patients with probable sporadic Creutzfeldt–Jakob disease: FDG-PET study using SPM and individual patient analysis

Dimitri Renard · Rik Vandenberghe · Laurent Collombier · Pierre-Olivier Kotzki · Jean-Pierre Pouget · Vincent Boudousq

Abstract Only one large series using statistical parametric mapping (SPM) reports on FDG-PET in sporadic (Heidenhain and non-Heidenhain variant) Creutzfeldt–Jakob disease (sCJD), describing hypometabolism in bilateral parietal, frontal, and occipital cortices. Our aim was to study FDG-PET in non-Heidenhain probable sCJD patients in order to assess the most pertinent FDG-PET pattern, and to compare FDG-PET and MRI data. We used both SPM and NeuroGam® software analysis, compared with healthy controls, to describe the FDG-PET abnormalities. Individual FDG-PET and MRI–DWI data were compared. SPM group analysis showed lateralized hypometabolism in the medial parietal cortex, the lateral and medial frontal (sparing Brodmann's area 4 and 6 and the anterior cingulate cortex), and lateral parietal cortex, in the absence of basal ganglia or cerebellar hypometabolism. The most severe hypometabolism was seen in Brodmann's area 31, and to a lesser degree area 23 (both areas correspond to the posterior cingulate cortex) and the precuneus. On individual analysis using NeuroGam® software, additional variable temporal cortex and frequent basal ganglia (with caudate nucleus as the most frequently involved structure) hypometabolism was seen, in the absence of cerebellar hypometabolism. The cerebral lobe cortex was more frequently and more severely hypometabolic than basal ganglia structures. Concordance between FDG-PET and MRI abnormalities was most often present for both the cerebral lobe cortex and the basal ganglia. In the case of discordance, FDG-PET was more sensitive than MRI for the cortex, whereas MRI was more sensitive than FDG-PET for the basal ganglia. When pathological, both cortical lobe cortex and basal ganglia involvement were slightly more often lateralized on FDG-PET than on MRI. Despite the presence of overlapping features with other diseases presenting with rapidly progressive dementia, the FDG-PET pattern we found in our non-Heidenhain sCJD patients may help in the differential diagnosis of rapidly progressive dementia.

Keywords Creutzfeldt–Jakob disease · [^{18}F]Fluoro-2-deoxy-D-glucose positron emission tomography · PET · MRI

D. Renard (✉)
Department of Neurology, CHU Nîmes, Hôpital Caremeau, Place du Pr Debré, 30029 Nîmes Cedex 4, France
e-mail: dimitrirenard@hotmail.com

R. Vandenberghe
Department of Neurology, University Hospitals Leuven, Herestraat 49, 3000 Leuven, Belgium

L. Collombier · P.-O. Kotzki · V. Boudousq
Department of Nuclear Medicine, CHU Nîmes, Hôpital Caremeau, Place du Pr Debré, 30029 Nîmes Cedex 4, France

J.-P. Pouget
Institut de Recherche en Cancérologie, INSERM U896, CRLC Val d'Aurelle, 34298 Montpellier Cedex 5, France

Introduction

Creutzfeldt–Jakob disease (CJD) is characterized by rapidly progressive dementia, a variety of neurological symptoms, and a fatal outcome. Pre-mortem diagnosis is based on the presence of clinical signs (dementia, ataxia, visual signs, pyramidal signs, extrapyramidal signs, akinetic mutism), periodic sharp wave complexes (PSWC) on electroencephalogram (EEG), 14-3-3 protein detection in the cerebrospinal fluid (CSF), and high signal in the basal ganglia or the temporal–parietal–occipital (at least two

regions have to be involved) cortex on diffusion-weighted imaging (DWI) or fluid-attenuated inversion recovery (FLAIR) MRI images [1]. Signal changes are more often seen on DWI than on FLAIR sequences [1].

There are relatively few reports (most are case reports) on [18F]fluoro-2-deoxy-D-glucose (FDG)-positron emission tomography (PET) in CJD, reporting widespread cerebral and rarely also cerebellar hypometabolism [2–9]. In a study of Xing et al. [9] (reporting five biopsy-proven and nine probable CJD patients), a high level of concordance between FDG-PET and MRI abnormalities was seen, with FDG-PET showing hypometabolism in extra brain areas (i.e. normal on MRI) suspecting FDG-PET changes to precede MRI abnormalities. Only one series, including six non-Heidenhain and five Heidenhain variant patients, used statistical parametric mapping (SPM) analysis to compare the glucose metabolism of sporadic Creutzfeldt–Jakob disease (sCJD) patients with normal controls [10]. In that study, non-Heidenhain sCJD patients showed decreased glucose metabolism in the bilateral parietal, frontal, and occipital cortices with right-sided predominance, in the absence of basal ganglia or cerebellar hypometabolism. The concordance between FDG-PET and MRI abnormalities was not studied in that report.

Our aim was to study FDG-PET brain metabolism and to assess the most hypometabolic area in non-Heidenhain variant probable sCJD patients using SPM. We also used commercially neurostatistical parametric mapping software (NeuroGam, Segami Corp.) for individual patient per patient analysis. This software allowed a regional metabolism analysis expressed as average Z-scores from an expected age-matched control normal population. The distribution of individual FDG-PET and MRI abnormalities were also analyzed in each patient. Both SPM and individual NeuroGam software analysis were used in order to find the most pertinent FDG-PET pattern.

Methods

Subjects

Amongst ten consecutive patients with non-Heidenhain variant sCJD recruited at the Department of Neurology, CHU Nîmes, Hôpital Caremeau, France between October 2007 and January 2013, nine patients (five men and four women) underwent both brain FDG-PET and MRI. All nine included and analyzed patients had clinically probable sCJD based on both the WHO criteria and the in 2009 updated clinical diagnostic criteria for sCJD [1]. None of our patients had initial visual symptoms, classically seen in Heidenhain variant CJD. Autopsy was not performed in our patients. Since we were also interested in the glucose metabolism of the basal ganglia and the cerebellum, special attention was paid to clinical extrapyramidal and cerebellar signs during hospitalisation.

Patient characteristics, EEG and CSF data, disease duration at time of the first analyzed brain imaging (FDG-PET or MRI), extrapyramidal and cerebellar signs, and codon 129 polymorphisms are shown in Table 1.

The mean age, at the moment of symptom onset, was 72 years (range 52–86). All patients, except two (showing only lateralized frontal and temporal slowing, respectively), showed PSWCs on EEG. All patients had CSF 14-3-3 protein. The mean time interval between symptom onset and first analyzed brain imaging was 62 days (range 18–126). Seven of our nine patients had signs interpreted as probable extrapyramidal in origin. The following signs were not interpreted as extrapyramidal signs: predominant kinetic intention tremor (interpreted as a cerebellar sign), alien limb sign (interpreted as cortical or callosal dysfunction), and myoclonus (interpreted as cortical dysfunction).

Seven out of our nine patients underwent (and two patients refused) genotyping of the prion protein gene (PRNP). Codon 129 polymorphism demonstrated methionine homozygosity in five patients and valine homozygosity in two patients. The mean total disease duration between symptom onset and dead was 127 days (range 37–378).

FDG-PET imaging (SPM analysis and individual analysis using NeuroGam)

FDG-PET was performed shortly before or after MRI (ranging from FDG-PET performed 8 days before MRI, to FDG-PET performance 16 days after MRI).

All brain FDG-PET scans were performed with a PET-CT GEMINI GXL (Philips Medical Systems). After fasting for at least 6 h, blood glucose level was <160 mg/dl. Patients were positioned comfortably in a quiet, dimly lit room before FDG administration and during the uptake phase of FDG (at least 20 min). They received intravenous injection of 185–250 MBq (5–6.7 mCi: according to the weight) of 18F-FDG by a canula inserted 10 min before. Patients were instructed not to speak, read or be otherwise active. For imaging, patients were in supine position, and the head immobilized in a masthead. Imaging began by CT surview (view angle 90, 120 kV, 30 mAs), then transmission CT scan for attenuation correction was done (120 kV, Mas/slice 200, Pitch 0.563, Rotation 1.5, thickness 3 mm, filter UB, collimation 16 × 1.5, FOV 600); static emission scan started 30 min after injection, in 3-D mode for 20 min, axial field of view 180 mm, 256 × 256 matrix, voxel size 2 mm^3, and reconstruction was done with a three dimensional row-action maximum likelihood algorithm LOR-RAMLA resulted in 90 transaxial slices.

Table 1 Patient characteristics, EEG and CSF data, disease duration at time of the first analyzed brain imaging (FDG-PET or MRI), extra-pyramidal and cerebellar signs, and codon 129 polymorphisms of the nine included patients

Patient no.	Sex	Age (years)	PSWC	14-3-3	Duration (days)	Extrapyramidal signs	Ataxia	Codon 129
1	M	79	+	+	18	Rigidity and dystonia	–	NP
2	M	79	+	+	51	Bradykinesia Right arm dystonia, Shuffling gait	+	Met/Met
3	M	69	–	+	105	Postural tremor	–	Val/Val
4	F	52	+	+	77	Right arm chorea Monotone speech	+	Met/Met
5	M	63	+	+	27	None	–	Met/Met
6	M	86	+	+	66	Right arm dystonia Shuffling gait	+	Met/Met
7	F	79	+	+	37	None	–	NP
8	F	70	–	+	53	Shuffling gait	+	Val/Val
9	F	75	+	+	126	Right arm dystonia	–	Met/Met

PSWC periodic sharp wave complexes, *Duration* disease duration at time of the first analyzed brain imaging, *Met/Met* methionine homozygosity at codon 129 in prion protein gene, *Val/Val* valine homozygosity at codon 129 in prion protein gene, *NP* not performed

Whereas NeuroGam software used native images, an Analyze format conversion was necessary before using SPM Software. The conversion was done using Xmedcon software, (http://xmedcon.sourceforge.net/). SPM2 software (Wellcome Department of Imaging Neuroscience, London; http://www.fil.ion.ucl.ac.uk/spm) running on Matlab 6.1 version (The Mathworks Inc., USA) running on Windows XP. Images were realigned and spatially normalized into the Montreal Neurological Institute (MNI, McGill University, Montreal, QC, Canada) standard template given by SPM software using affine and non-linear transformation. Images were reformatted to a final voxel size of $2 \times 2 \times 2$ mm and smoothed using an isotropic Gaussian kernel of $12 \times 12 \times 12$ mm FWHM for the main analyses performed.

For basal ganglia analysis, in the literature, a Gaussian kernel of $6 \times 6 \times 6$ mm FWHM is more commonly used. Therefore, for SPM analysis, an additional analysis using a Gaussian kernel of $6 \times 6 \times 6$ mm FWHM was performed.

A global normalization for voxel count was performed using a proportional scaling. The gray-level threshold was set to 0.8, i.e. only voxels with an intensity level above 0.8 of the mean level for that scan were included in the statistical analysis. Statistical comparisons between groups were performed on a voxel-by-voxel basis t statistics, generating SPM (t) maps. We investigated hypometabolic brain areas, a stringent level of significance of $p < 0.05$ corrected for multiple comparisons (SPM family wise error—FWE) was adopted with an extent threshold of 100 voxels. For visualization, the significant voxels were projected onto the 3-D rendered brain or a standard MRI template allowing anatomic identification. Anatomical loci

were also determined by converting cluster maxima to Talairach space ([11]; http://imaging.mrc-cbu.cam.ac.uk/imaging/MniTalairach). This output was cross-checked using the atlases of Talairach and Tournox [11]. Three comparisons were done (1) total sCJD patients versus controls, (2) the six sCJD patients with a visualized left predominant cerebral hypometabolism versus controls, (3) the three sCJD patients with a visualized right predominant cerebral hypometabolism versus controls. For SPM analysis, the control group consisted of 36 subjects (mean age 62 years) who had neither a history of neurological and psychiatric illness nor abnormalities on neurological examination.

Individual brain PET study was quantified and compared to an age-matched normal database using NeuroGam Software (GE Medical Systems; Segami Corporation, Columbia, MD, USA). This software applies an affine anatomical coregistration by blocks of data defined in the Talairach space. An anatomical standardization and a voxel value normalization to the cerebral maximum value was done. Patient and subjects control database comparison was done voxel by voxel in the brain cortex and the basal ganglia creating a Z-score map [12].

The Z-score maps were displayed either in the standard cuts or by overlay on a 3-D anatomical topographic representation by means of a specific colour scale. For NeuroGam analysis, the reference population contained: 28 controls for 50–60 year-old patients (sex ratio men/women = 1.54), 30 controls for 60–70 year-old patients (sex ratio 1.72), 31 controls for 70–80 year-old patients (sex ratio 1.21), and six controls for 80–90 year-old patients (sex ratio 2). For individual patient analysis using

NeuroGam software, we studied semi-quantitatively intra- and inter-individual differences in metabolism in the cerebral and cerebellar cortex using 3-D reconstruction FDG-PET images (considering the four different cerebral lobes, i.e. the frontal, the parietal, the occipital, and the temporal lobes; and each cerebellar hemisphere), and the basal ganglia using axial views (considering the caudate nucleus, the lentiform nucleus, and the thalamus). A cerebral cortical lobe, a cerebellar cortical hemisphere, or a basal ganglia substructure was considered hypometabolic when a clear zone of hypometabolism of more than 2 standard deviations (SD) was found. For each cerebral cortical lobe, hypometabolism was called slight when <50 % of the surface of the involved lobe showed a hypometabolism of more than 2 SD, and called severe when more than 50 % of the surface showed hypometabolism of more than 2 SD. Lobes showing hypometabolism less severe than 2 SD were called 'normal'. To study lateralization of the cerebral lobe involvement in a given patient, hypometabolism in the concerned lobe was considered lateralized when one side was hypometabolic and the other side normal (i.e. no areas with hypometabolism of >2 SD), or when the involved (>2 SD) area exceeded by 30 % or more the involved (>2 SD) area in the contralateral lobe. In cases where bilateral extensive lobe hypometabolism was present with the least involved lobe showing >2 SD hypometabolism in more than 70 % of its lobe surface, lateralization was considered present when one lobe showed more than 30 % of lobe surface with >3 SD hypometabolism when compared with the opposite side.

For the basal ganglia, based on axial views this time, the same criteria as stated for the cerebral cortex for distinction between slight and severe involvement and for lateralization were used.

MR imaging

As required by the in 2009 updated clinical diagnostic criteria for sCJD, all patients had hyperintense signal in the basal ganglia or in at least two cortical regions on DWI or FLAIR sequences. In our study, only DWI images were analysed. For each cerebral cortical lobe, MRI involvement was called slight when <50 % of the lobe surface showed DWI hyperintensity, and called severe when DWI hyperintensity involved >50 % of the lobe surface. MRI involvement was considered lateralized when one lobe was involved and the contralateral lobe normal, or when the involved area exceeded by 30 % or more the involved area in the contralateral lobe (in case of bilateral lobe MRI involvement). In our MRI analysis, only each lobe as a whole was considered, and thus no specific cortical areas were assessed. When radiologically involved in CJD, basal ganglia substructure involvement is typically diffuse,

showing gradients of hyperintensity. Therefore, severity as such was not scored in case of basal ganglia involvement, and for lateralization assessment was based on the hyperintensity of the involved basal ganglia substructure (i.e. lateralization was considered present when hyperintensity existed on one side associated with normal contralateral signal or when one side showed clearly a DWI signal more intense than on the contralateral side).

FDG-PET and MRI concordance

In each patient, concordance of the FDG-PET and MRI abnormalities was analysed using NeuroGam and MRI-DWI images of each patient.

Results

FDG-PET SPM group analysis

Compared with controls, SPM analysis in our nine sCJD patients showed hypometabolism in the medial parietal cortex bilaterally, and in the left-sided lateral and medial frontal (sparing Brodmann's area 4 and 6, and the anterior cingulate cortex) and the lateral parietal cortex (Fig. 1). The brain area showing the most severe hypometabolism was Brodmann's area 31 and to a lesser degree Brodmann's area 23 (both areas correspond to the posterior cingulate cortex) and the precuneus. SPM analysis did not reveal basal ganglia or cerebellar hypometabolism. Basal ganglia hypometabolism was also absent on additional SPM analysis using a Gaussian kernel of $6 \times 6 \times 6$ mm FWHM.

When present, cortical hypometabolism was lateralized in each lobe on individual patient analysis, resulting potentially in an underestimation of lateralized hypometabolism when confounding patients with different side predominance of hypometabolism. Therefore, we also performed separate SPM analysis in the group with left-sided predominant hypometabolism ($n = 6$) and in the group of patients with right-sided predominant hypometabolism ($n = 3$). In each of these groups, SPM analysis continued to show the posterior cingulate cortex (bilateral but predominant on the left side in the left-sided predominant group, and almost strictly unilateral on the right side in the right-sided predominant group) as the most hypometabolic area (Fig. 2). In the group with left-sided predominant hypometabolism, associated lateral and medial frontal and lateral parietal cortex hypometabolism involved larger areas extending into the lateral posterior temporal cortex (Fig. 2), whereas in the group with right-sided predominant hypometabolism only small zones of associated lateral frontal hypometabolism were seen (Fig. 2).
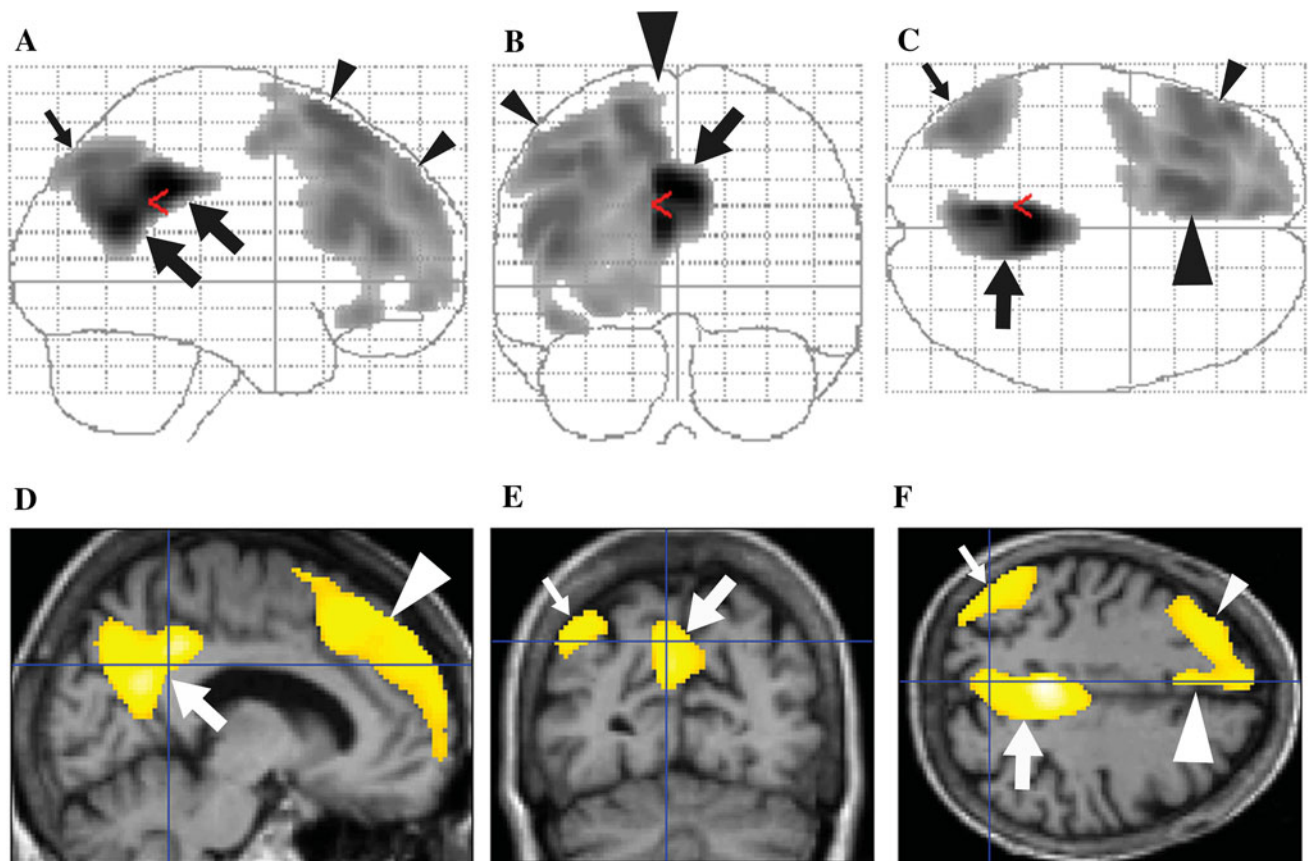
Fig. 1 Compared with controls, SPM analysis (**a** and **d** are sagital views, **b** and **e** coronal views, and **c** and **f** axial views) in our nine sCJD patients showing the most severe hypometabolism in Brodmann's area 31 (**a–f** *large arrows*) and to a lesser degree Brodmann's area 23 and the precuneus, associated with hypometabolism in the left-sided lateral (**a, b, c**, and **f**, *small arrowheads*) and medial (**b, c, d**, and **f**, *large arrowheads*) frontal and lateral parietal (**a, c, e**, and **f**, *small arrows*) cortex

FDG-PET individual patient analysis using NeuroGam

Semi-quantitative data of cerebral cortical and basal ganglia FDG-PET metabolism are shown in Tables 2 and 3. When considering the cortex of the four different lobes in each hemisphere in each patient, 49 out of 72 lobes (68 %) were hypometabolic (including 28 lobes with slight and 21 lobes with severe involvement) on FDG-PET, leaving one frontal, four temporal, four parietal, and 14 occipital lobes with normal metabolism. Lateralization was seen in 29 of the 36 lobes (81 %). The remaining seven lobes without lateralization did not show hypometabolism. Thus, when present, cortical lobe hypometabolism was never symmetrical.

The shared FDG-PET pattern of hypometabolic cortical zones in all patients was asymmetrical hypometabolism in the medial parietal lobe, the lateral and medial frontal lobe (typically sparing the Brodmann's area 4 and 6, and the anterior cingulate cortex), and to a lesser degree the lateral parietal lobe. Associated variable temporal lobe hypometabolism was also seen. Hypometabolism in the lateral parietal lobe was less severe or involved smaller areas than in the medial parietal lobe and the frontal lobe except in one patient (patient 3, showing

profound lateral parietal hypometabolism). Associated temporal hypometabolism was less severe than in the medial parietal and the frontal lobe in five patients, equally severe in three, and more severe in one patient (patient 3).

FDG-PET metabolism in the basal ganglia was significantly decreased in 12 (with 11 with slight and one with severe involvement) out of 54 (22 %) basal ganglia structures (i.e. considering caudate nucleus, lentiform nucleus, and thalamus of each hemisphere in each patient), corresponding to 6 patients showing basal ganglia hypometabolism (all lateralizing to the side of the predominant cortical hypometabolism) with the caudate nucleus as the most frequently involved hypometabolic basal ganglia substructure. When basal ganglia substructure hypometabolism was present, lateralization was found in all.

None of the patients had cerebellar hypometabolism.

Individual MRI analysis

Semi-quantitative MRI data of the cortex and the basal ganglia are shown in Tables 2 and 3. When considering the cortex of the four different lobes in each hemisphere in each
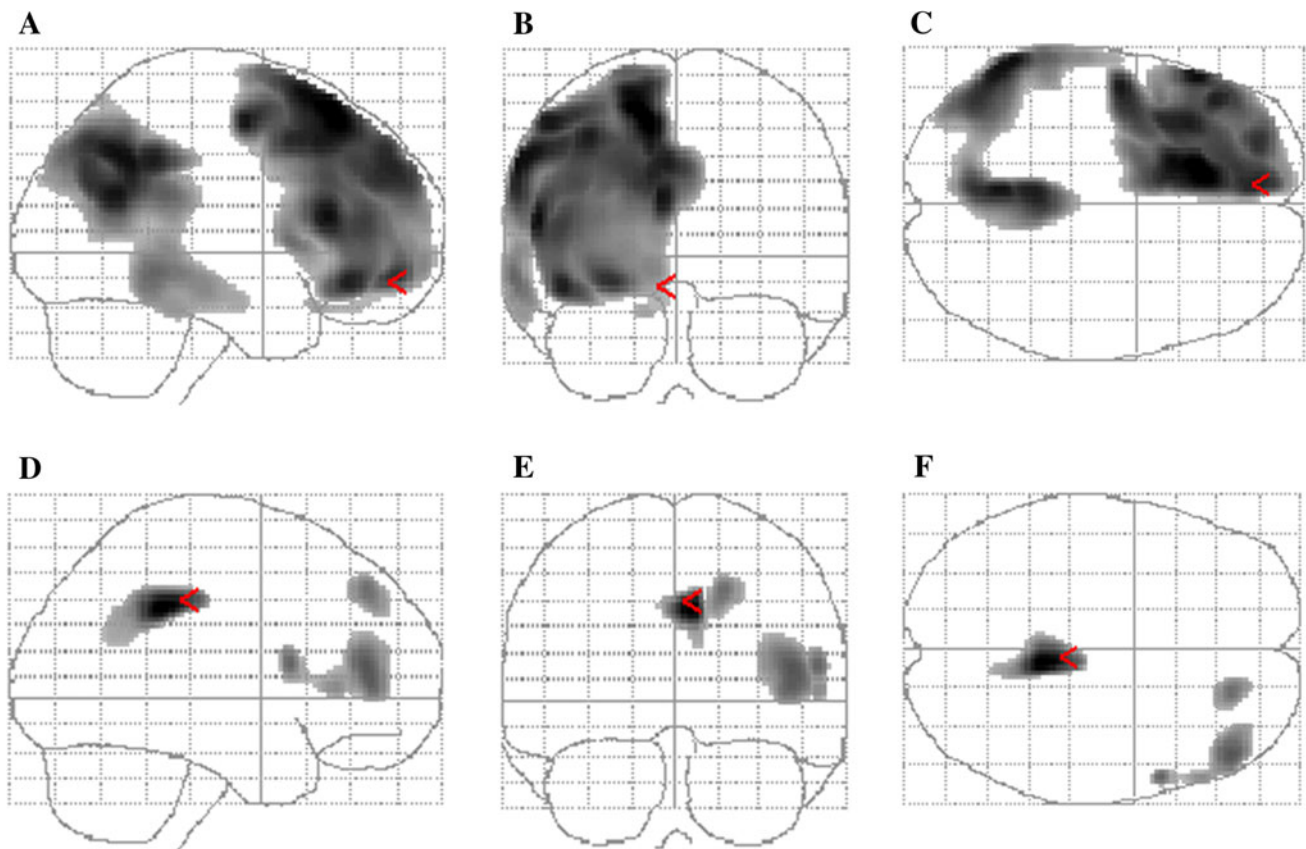
Fig. 2 SPM analysis in the group with left-sided predominant hypometabolism (**a–c**) and in the group of patients with right-sided predominant hypometabolism (**d–f**) continued to show medial parietal cortex hypometabolism in both groups. In the group with left-sided predominant hypometabolism, associated lateral and medial frontal and lateral parietal cortex hypometabolism involves larger areas extending into the lateral posterior temporal cortex (**a–c**), whereas in the group with right-sided predominant hypometabolism only small zones of associated lateral frontal hypometabolism is seen (**d–f**)

patient, 46 (27 with slight and 19 with severe involvement) out of 72 lobes (64 %) were abnormal on MRI (leaving 11 occipital, six temporal, six parietal, and four frontal lobes with normal MRI). Lateralization was seen in 24 of the 36 lobes (67 %). The remaining 12 lobes without lateralization included five lobes with (and thus symmetrical) hypometabolism and seven lobes without hypometabolism.

Basal ganglia MRI signal abnormalities were seen in 18 out of 54 basal ganglia structures (33 %), corresponding to five out of nine patients showing basal ganglia abnormalities, with the caudate nucleus as the most frequently involved structure. When basal ganglia DWI hyperintensity was seen ($n = 10$), involvement was asymmetrical in eight and symmetrical in two cases.

FDG-PET (using NeuroGam) and MRI concordance in individual patient analysis

When analysing the cortex of all 72 lobes, MRI and FDG-PET side concordance was found in 51/72 (71 %) lobes (both pathological MRI and FDG-PET for the concerned lobe $n = 37$, both normal $n = 14$) and discordance was seen in 21/72 lobes (with nine lobes where MRI abnormalities were seen in absence of FDG-PET changes, and 12 lobes showing FDG-PET hypometabolism without MRI abnormalities). When lateralization was present on MRI (unilateral or bilateral lateralized cortical hyperintensity $n = 24$), FDG-PET side concordance was present (with unilateral or bilateral lateralized hypometabolism, ipsilateral to the predominant MRI abnormalities) in $n = 21$ lobes (87.5 %).

Concordance between MRI and FDG-PET abnormalities was seen in 34 out of 54 (63 %) basal ganglia substructures (both pathological five and both normal 29). PET hypometabolism was seen in absence of MRI abnormalities in seven substructures, and vice versa in 13 substructures. There was no clear concordance between the presence of clinical extrapyramidal signs and FDG-PET/MRI basal ganglia abnormalities.

Discussion

Using SPM in our nine non-Heidenhain variant sCJD patients, the FDG-PET pattern we found was lateralized

Table 2 Semi-quantitative data of cerebral cortical MRI abnormalities and FDG-PET changes

Nr R/L	MRI-front R/L	FDG-front R/L	MRI-par R/L	FDG-par R/L	MRI-oc R/L	FDG-oc R/L	MRI-temp R/L	FDG-temp
1	+/+ (sym)	++/++ (R > L)	++/++ (sym)	++/++ (R > L)	–/–	++/++ (R > L)	++/++ (sym)	++/+
2	+/+ (L > R)	+/++	++/++ (L > R)	+/++	+/+ (sym)	–/–	+/+ (L > R)	–/+
3	++/++ (sym)	++/+	–/–	++/+	–/–	–/–	+/–	++/+
4	++/+	–/+	–/+	–/+	–/–	–/–	–/+	–/+
5	+/+ (L > R)	+/+ (L > R)	–/+	–/+	–/++	–/–	–/+	–/+
6	–/++	+/++	+/++	–/+	+/++	–/–	–/+	+/+ (L > R)
7	–/–	++/++ (R > L)	+/++	++/++ (R > L)	+/+ (R > L)	+/+ (R > L)	+/++	+/+ (L > R)
8	+/+ (L > R)	+/++	–/+	–/+	–/–	–/–	+/++	–/++
9	–/++	+/++	–/++	+/++	–/–	–/–	–/++	+/+ (L > R)

Nr patient number, *front* cortical frontal lobe involvement, *par* cortical parietal lobe involvement, *oc* cortical occipital lobe involvement, *temp* cortical temporal lobe involvement, *R* right-sided, *L* left-sided, *sym* symmetrical, + slight involvement corresponding to DWI hyperintensity involving less than 50 % of the lobe surface on MRI and corresponding to <50 % of the involved lobe showing >2 SD FDG-PET hypometabolism, ++ severe involvement corresponding to DWI hyperintensity seen in more than 50 % of the lobe surface on MRI and corresponding to more than 50 % of the lobe surface showing >2 SD FDG-PET hypometabolism. In cases of bilateral slight or severe involvement, lateralization was noted for the involved lobe when present

hypometabolism in the inferior region of the medial parietal cortex (corresponding to the most hypometabolic area), and the lateral and medial frontal and lateral parietal cortex. On SPM, hypometabolic zones were larger in patients with left-sided predominant hypometabolism than in patients with right-sided predominant hypometabolism. This might be explained by the larger number of patients with left-sided predominant hypometabolism in our study. Hypometabolism lateralizing to the left side in our study was in contrast with the right-sided predominance found by Kim et al. [10]. This may be explained by the small sample size of both studies.

In our study, SPM analysis did not show basal ganglia hypometabolism.

In general, reduced FDG-PET signal is due to reduced metabolism and/or brain volume loss. Our FDG-PET data were not partial volume corrected, so it can not be determined to what degree the reduced FDG-PET signal was related to true hypometabolism or related to focal brain volume loss. MRI scans were mainly performed according to a clinical protocol, and no formal volumetric analysis of the MRI data was performed.

On individual patient analysis, cerebral lobe cortex was more frequently and more severely hypometabolic than basal ganglia structures. FDG-PET hypometabolism was slightly more frequent than DWI hyperintensity in the cortical lobes, whereas basal ganglia structures showed MRI abnormalities more frequently than FDG-PET changes. Concordance between FDG-PET and MRI abnormalities was most often present for both the cerebral lobe cortex and the basal ganglia. In cases of discordance, FDG-PET was more sensitive than MRI for the cortex, whereas MRI was more sensitive than FDG-PET for the basal ganglia. When pathological, both cortical lobe cortex and basal ganglia involvement were slightly more often lateralized on FDG-PET than on MRI.

Our findings about FDG-PET and MRI abnormalities in CJD are difficult to compare with the data reported by Xing et al. since in their report no details are given about the methodology used to analyse FDG-PET and MRI abnormalities. However, with the methods we used, superiority of sensitivity of FDG-PET compared to MRI was not as evident as suggested by Xing et al. in their report. On FDG-PET the caudate nucleus was the most frequently involved basal ganglia structure, corresponding well to the anterior predominance of basal ganglia MRI changes earlier reported in sCJD [13]. MRI and FDG-PET seem to represent, at least partly, distinct pathophysiological processes in sCJD. Discordance is even more important when comparing our FDG-PET data (with relatively focal and asymmetrical abnormalities) with the earlier reported pathological brain changes showing quite diffuse and symmetrical involvement [14, 15]. Reports on sCJD cases describe widespread brain vacuolation (spongiform change) and prion (PrP) deposition, with the hippocampus and the dentate gyrus as the least involved areas, in absence of clear asymmetry. The density of vacuolation and the level of PrP deposition were not correlated in most of the brain areas, with the occipital cortex yielding the highest density of vacuolation (followed by the frontal and parietal cortex) while the parietal cortex (followed by the parahippocampal gyrus and the inferior temporal gyrus) showed the highest PrP deposition [15].

The FDG-PET pattern we found in our non-Heidenhain variant sCJD patients may help in the differential diagnosis of rapidly progressive dementia such as frontotemporal dementia, progressive supranuclear palsy, Alzheimer's disease, corticobasal degeneration, dementia with Lewy bodies, autoimmune or paraneoplastic encephalitis, and brain cancer (especially lymphoma) [16]. For instance, in Alzheimer's disease, FDG-PET hypometabolism is most often seen in the parietal lobe (including the precuneus)

Tale 3 Semi-quantitative data of basal ganglia MRI and FDG-PET abnormalities

Nr	MRI-BG	FDG-BG
	R/L	R/L
1	CN −/−	CN ++/−
	LN −/−	LN −/−
	Thal −/−	Thal +/−
2	CN −/+	CN −/−
	LN −/−	LN −/−
	Thal −/−	Thal −/−
3	CN −/−	CN +/−
	LN −/−	LN +/−
	Thal −/−	Thal −/−
4	CN +/+ (sym)	CN −/−
	LN +/+ (L > R)	LN −/−
	Thal −/−	Thal −/−
5	CN −/−	CN −/−
	LN −/−	LN −/−
	Thal −/−	Thal −/−
6	CN −/−	CN −/+
	LN −/−	LN −/+
	Thal −/−	Thal −/+
7	CN +/+ (R > L)	CN +/−
	LN +/−	LN −/−
	Thal −/−	Thal −/−
8	CN +/+ (L > R)	CN +/+ (L > R)
	LN +/+ (L > R)	LN −/+
	Thal +/+ (sym)	Thal −/−
9	CN +/+ (L > R)	CN −/+
	LN +/+ (L > R)	LN −/−
	Thal −/−	Thal −/−

Nr patient number, *BG* basal ganglia, *CN* caudate nucleus, *LN* lentiform nucleus, *Thal* thalamus, *R* right-sided, *L* left-sided, *sym* symmetrical

For the MRI results, + corresponds to the presence of diffuse DWI hyperintensity of the involved BG substructure. In case of bilateral involvement, lateralization was noted for the involved structure

For the FDG-PET data, + corresponds to the presence of <50 % of the involved BG substructure showing >2 SD hypometabolism, and ++ corresponds to the presence of more than 50 % of the involved BG substructure showing >2 SD hypometabolism. In cases of bilateral slight or severe involvement, lateralization was noted for the involved structure when present

and the temporal lobe (especially the medial part), while the frontal lobe is typically less or later involved. In dementia with Lewy bodies, hypometabolism of the occipital and temporoparietal (including the precuneus and the posterior cingulate gyrus) cortex is most frequently seen together with relative hypermetabolism of putamen and pallidum. In progressive supranuclear palsy, hypometabolism is typically seen in the midline frontal cortex

together with caudate nucleus, thalamic, and upper brainstem involvement. In frontotemporal dementia, frontal and anterior temporal cortex hypometabolism is typically seen with milder parietal lobe hypometabolism. As opposed to what was seen in our sCJD patients, the behavioural variant frontotemporal dementia shows severe orbitofrontal and anterior cingulate cortex hypometabolism. In these degenerative diseases, lateralization is classically not as severe as observed in our sCJD patients, except for corticobasal degeneration were hypometabolism is often very asymmetrical involving essentially the parietal cortex (possibly extending into the perirolandic area, which was typically spared in our sCJD patients) and the striatum, and for progressive nonfluent aphasia (another frontotemporal dementia subtype) with typical asymmetric (lateralized to the left side) frontotemporal hypometabolism.

The posterior cingulate cortex, and to a lesser degree the precuneus, were the most hypometabolic brain area in our sCJD patients. Posterior cingulate and precuneus are also among the areas of predilection in the early stages of Alzheimer's disease, both with regards to MRI volume loss, FDG-PET hypometabolism, and amyloid deposition [17–20]. For posterior cingulate and precuneus this has been linked to their status as a network hub, including their centrality in the connections from the hippocampal formation to parietal cortex [21–24]. Our findings show that precuneus hypometabolism is not specific for Alzheimer's disease. Most distinctive in comparison to Alzheimer's disease appears to be the absence of posterior and inferior temporal hypometabolism and the absence of inferior lateral parietal hypometabolism in the presence of strong prefrontal and medial parietal involvement. This, however, would require validation in an independent dataset.

The precuneus probably plays a central role in a wide spectrum of highly integrated tasks including visuo-spatial imagery, self-processing operations, episodic memory retrieval (especially with autobiographical content), and consciousness [25]. The precuneus shows one of the highest metabolic patterns of all brain areas during the conscious resting state, and selective hypometabolism in the precuneus has been reported in several states associated with altered consciousness, such as sleep, drug-induced anaesthesia, hypnotic state, and vegetative states. Precuneus and posterior cingulate cortex are both involved in non rapid eye movement sleep, and their dysfunction in sCJD might be implicated in the sleep-wake disturbances earlier reported in sCJD, especially since in some of the reported sCJD cases no prominent thalamic (corresponding to the structure most often involved when for instance disappearance of EEG spindles frequency activity is seen) neurodegeneration was found and thalamic FDG-PET hypometabolism was seen in only two of our sCJD patients [26, 27]. Further clinical evaluation is needed in early stage

sCJD patients in order to analyse if the FDG-PET hypometabolism in the posterior cingulate cortex (i.e. the most hypometabolic area in our patients) corresponds to specific neuropsychological dysfunction.

All our patients, at the time of FDG-PET evaluation, fulfilled the clinical probable CJD criteria. It is unknown if the described FDG-PET abnormalities are also present early in the disease, preceding MRI, CSF, or EEG abnormalities. Patients with suspected sCJD have to be analysed in early stage disease (when classical clinical diagnostic criteria often lack and other differential diagnoses are considered) in order to see if FDG-PET can help to make an earlier and reliable diagnosis of sCJD.

A major drawback in our study is that no neuropathological analyses were performed to confirm the diagnosis of CJD. To further analyse the true value of FDG-PET in CJD patients, several groups of patients presenting with rapidly progressive dementia (with proven neuropathological diagnosis at the end) should be studied prospectively by FDG-PET.

Conclusion

Despite the presence of overlapping features with other diseases presenting with rapidly progressive dementia, the FDG-PET pattern we found, i.e. lateralized hypometabolism in the medial parietal cortex (with Brodmann's area 31 as the most hypometabolic area, followed by Brodmann's area 23 and the precuneus) and the lateral and medial frontal and lateral parietal cortex, in our non-Heidenhain sCJD patients may help in the differential diagnosis of rapidly progressive dementia.

Conflicts of interest   We have no conflict of interest to declare.

Ethical standard   This study has been approved by the appropriate ethics committee and have therefore been performed in accordance with the ethical standards laid down in the 1964 Declaration of Helsinki and its later amendments. All persons gave their informed consent prior to their inclusion in the study.

References

1. Zerr I, Kallenberg K, Summers DM et al (2009) Updated clinical diagnostic criteria for sporadic Creutzfeldt–Jakob disease. Brain 132:2659–2668
2. Na DL, Suh CK, Choi SH et al (1999) Diffusion-weighted magnetic resonance imaging in probable Creutzfeldt–Jakob disease: a clinical-anatomic correlation. Arch Neurol 56:951–957
3. Engler H, Lundberg PO, Ekbom K et al (2003) Multitracer study with positron emission tomography in Creutzfeldt–Jakob disease. Eur J Nucl Med Mol Imaging 30:85–95
4. Holthoff VA, Sandmann J, Pawlik G et al (1990) Positron emission tomography in Creutzfeldt–Jakob disease. Arch Neurol 47:1035–1038
5. Friedland RP, Prusiner SB, Jagust WJ et al (1984) Bitemporal hypometabolism in Creutzfeldt–Jakob disease measured by positron emission tomography with [^{18}F]-2-fluorodeoxyglucose. J Comput Assist Tomogr 8:978–981
6. Goldman S, Laird A, Flament-Durand J et al (1993) Positron emission tomography and histopathology in Creutzfeldt–Jakob disease. Neurology 43:1828–1830
7. Matochik JA, Molchan SE, Zametkin AJ et al (1995) Regional cerebral glucose metabolism in autopsy-confirmed Creutzfeldt–Jakob disease. Acta Neurol Scand 91:153–157
8. Fujita K, Harada M, Sasaki M et al (2012) Multicentre multiobserver study of diffusion-weighted and fluid-attenuated inversion recovery MRI for the diagnosis of sporadic Creutzfeldt–Jakob disease: a reliability and agreement study. BMJ Open 30(2):e000649
9. Xing XW, Zhang JT, Zhu F et al (2012) Comparison of diffusion-weighted MRI with ^{18}F-fluorodeoxyglucose-positron emission tomography/CT and electroencephalography in sporadic Creutzfeldt–Jakob disease. J Clin Neurosci 19:1354–1357
10. Kim EJ, Cho SS, Jeong BH et al (2012) Glucose metabolism in sporadic Creutzfeldt–Jakob disease: a statistical parametric mapping analysis of (18) F-FDG PET. Eur J Neurol 19:488–493
11. Talairach J, Tournoux P (1988) Co-planar stereotaxic atlas of the human brain: 3-Dimensional proportional system—an approach to cerebral imaging. Thieme Medical, New York
12. Paschali A, Messinis L, Lyros E et al (2009) Neuropsychological functions and rCBF SPECT in Parkinson's disease patients considered candidates for deep brain stimulation. Eur J Nucl Med Mol Imaging 36:1851–1858
13. Vitali P, Maccagnano E, Caverzasi E et al (2011) Diffusion-weighted MRI hyperintensity patterns differentiate CJD from other rapid dementias. Neurology 76(20):1711–1719
14. Cali I, Castellani R, Yuan J et al (2006) Classification of sporadic Creutzfeldt–Jakob disease revisited. Brain 129:2266–2277
15. Armstrong RA, Cairns NJ, Lantos PL (2001) Quantification of the vacuolation (spongiform change) and prion protein deposition in 11 patients with sporadic Creutzfeldt–Jakob disease. Acta Neuropathol 102:591–596
16. Berti V, Pupi A, Mosconi L (2011) PET/CT in diagnosis of dementia. Ann N Y Acad Sci 1228:81–92
17. Herholz K, Salmon E, Perani D et al (2002) Discrimination between Alzheimer dementia and controls by automated analysis of multicenter FDG PET. Neuroimage 17:302–316
18. Mosconi L, Tsui WH, Herholz K et al (2008) Multicenter standardized ^{18}F-FDG PET diagnosis of mild cognitive impairment, Alzheimer's disease, and other dementias. J Nucl Med 49:390–398
19. Dickerson BC, Bakkour A, Salat DH et al (2009) The cortical signature of Alzheimer's disease: regionally specific cortical thinning relates to symptom severity in very mild to mild AD dementia and is detectable in asymptomatic amyloid-positive individuals. Cereb Cortex 19:497–510
20. La Joie R, Perrotin A, Barré L et al (2012) Region-specific hierarchy between atrophy, hypometabolism, and ß-amyloid (Aß) load in Alzheimer's disease dementia. J Neurosci 32:16265–16273
21. Buckner RL, Sepulcre J, Talukdar T et al (2009) Cortical hubs revealed by intrinsic functional connectivity: mapping, assessment of stability, and relation to Alzheimer's disease. J Neurosci 29:1860–1873
22. Mormino EC, Brandel MG, Madison CM et al (2012) Not quite PIB-positive, not quite PIB-negative: slight PIB elevations in

elderly normal control subjects are biologically relevant. Neuroimage 59:1152–1160

23. Mesulam MM, Van Hoesen GW, Pandya DN et al (1977) Limbic and sensory connections of the inferior parietal lobule (area PG) in the rhesus monkey: a study with a new method for horseradish peroxidase histochemistry. Brain Res 136:393–414

24. Seltzer B, Pandya DN (1994) Parietal, temporal, and occipital projections to cortex of the superior temporal sulcus in the rhesus monkey: a retrograde tracer study. J Comp Neurol 343:445–463

25. Cavanna AE, Trimble MR (2006) The precuneus: a review of its functional anatomy and behavioural correlates. Brain 129:564–583

26. Maquet P (2012) Understanding non rapid eye movement sleep through neuroimaging. World J Biol Psychiatry 11(Suppl 1):9–15

27. Landolt HP, Glatzel M, Blättler T et al (2006) Sleep-wake disturbances in sporadic Creutzfeldt–Jakob disease. Neurology 9(66):1418–1424